Reactions of $Co_2Rh_2(CO)_{12}$ with Isocyanides and 1-Alkynes. Characterization of New Isocyanide and 1-Alkyne Complexes of Co–Rh Mixed-Metal Systems and the Structures of $[Rh(C{\equiv}N\text{-}C_6H_3Me_2\text{-}2,6)_4][Co(CO)_4]$ and $Co_2Rh_2(CO)_7(\mu\text{-}CO)_2(\mu_4,\eta^2\text{-}HC{\equiv}CBu^n)(PPh_3)$

Iwao Ojima,* Núria Clos,[1] Robert J. Donovan, and Patrizia Ingallina[2]

Department of Chemistry, State University of New York at Stony Brook, Stony Brook, New York 11794

Received January 23, 1991

Reactions of $Co_2Rh_2(CO)_{12}$ with isocyanides and 1-alkynes are studied. With isocyanides, fragmentation of the tetranuclear framework into dinuclear units occurs to give a series of new mixed-metal dinuclear complexes, $CoRh(CO)_{7-n}(CN\text{-}Bu^t)_n$ (n = 1, 2) and $[Rh(CN\text{-}R)_4][Co(CO)_4]$ (R = Bu^t, cyclohexyl, 2,6-$Me_2C_6H_3$). In all cases, isocyanide ligands are exclusively bonded to the rhodium atom. The structure of $[Rh(C{\equiv}N\text{-}C_6H_3Me_2\text{-}2,6)_4][Co(CO)_4]$ is confirmed by X-ray crystallography, which crystallizes in monoclinic unit cell with space group $P2_1/c$ (a = 10.820 (2) Å, b = 16.3206 (9) Å, c = 21.646 (4) Å; β = 90.700 (7)°; Z = 4). Least-squares refinement led to a value for R of 0.032 (R_w = 0.039) and a goodness of fit of 1.52 for 3892 reflections with $I > 3\sigma(I)$. The rhodium moiety is square planar and the cobalt moiety is tetrahedral with slight distortion in both moieties. The Rh–Co distance is 3.3785 (9) Å, and one of the Co–CO bonds is eclipsed with one of the Rh—C≡N—R bonds. 1-Alkynes insert into the Co–Co bond of the tetranuclear cluster to give butterfly clusters, $Co_2Rh_2(CO)_{10}(HC{\equiv}CR)$ (R = Bu^n, Ph, $SiMe_3$). Triphenylphosphine complexes of the new 1-alkyne-bridged butterfly clusters, $Co_2Rh_2(CO)_{10-n}(HC{\equiv}CBu^n)(PPh_3)_n$ (n = 1, 2), $Co_2Rh_2(CO)_8(HC{\equiv}CPh)(PPh_3)_2$, and $Co_2Rh_2(CO)_9(HC{\equiv}CSiMe_3)(PPh_3)$, are also synthesized. IR, ^1H NMR, and ^{13}C NMR spectroscopic data and elemental analyses support the formulation of these complexes as butterfly structures and the X-ray crystal structure of $Co_2Rh_2(CO)_9(HC{\equiv}CBu^n)(PPh_3)$ is determined: triclinic, space group $P\bar{1}$ (a = 10.389 (5) Å, b = 17.40 (2) Å, c = 10.03 (2) Å; α = 105.9 (1)°, β = 103.7 (1)°, τ = 82.59 (6)°; Z = 2; R = 0.051 (R_w = 0.063); a goodness of fit = 1.73 for 4832 reflections with $I > 3\sigma(I)$.

Introduction

Mixed-metal clusters have high potential to serve as efficient catalysts for a variety of homogeneous catalytic reactions as well as unique reagents for organic syntheses. Following the identification of $CoRh(CO)_7$ as an active catalytic species in the hydroformylation–amidocarbonylation of pentafluorostyrene catalyzed by mixed-metal systems of cobalt and rhodium,[3] we have been investigating the catalytic activity and reactions of $Co_2Rh_2(CO)_{12}$ and $CoRh(CO)_7$ to explore unique properties of these mixed-metal systems. It has been shown that reactions of $Co_2Rh_2(CO)_{12}$ with nucleophiles such as carbon monoxide,[4,5] phosphines,[6-9] phosphites,[7,10] and weak Lewis bases[6] occur at the rhodium site, whereas reactions with diphenyl- and bis(pentafluorophenyl)acetylenes[11,12] take place at the cobalt site. It has also been reported that some reactions proceed with retention of the tetranuclear structure, while, in other cases, fragmentation to a dinuclear species with preferential retention of the cobalt–rhodium bond takes place. For example, replacement of carbonyl ligands in $Co_2Rh_2(CO)_{12}$ by trimethyl phosphite gave a mixture of substitution products, from which mono-, di-, and trisubstituted complexes of general formula, $[Co_2Rh_2(CO)_{12-n}(P(OMe)_3)_n]$ (n = 1–3), were isolated.[7] On the other hand, when the substitution reactions were carried out with triethylphosphine, fragmentation of the cluster was observed; viz., the mixed-metal cluster reacted with 1 and 2 equiv of PEt_3 to form the corresponding mono- and disubstituted tetranuclear clusters, respectively, but addition of more triethylphosphine led to the formation of a disubstituted dinuclear species, $CoRh(CO)_5(PEt_3)_2$. We have looked at the reactions of $Co_2Rh_2(CO)_{12}$ with isonitriles and 1-alkynes and also the substitution reaction of the resulting novel Co–Rh mixed-metal butterfly cluster incorporating 1-hexyne with triphenylphosphine. We describe here the full account of our research on this subject.

Results and Discussion

Reactions with Isocyanides. The reactions of $Co_2Rh_2(CO)_{12}$ with isocyanides were carried out to investigate (i) whether substitution would occur selectively at cobalt or rhodium and (ii) if this replacement would take place with retention of the cluster framework or with fragmentation into simpler units. FT-IR spectroscopy was used to follow the course of the substitution reactions with

(1) Present address: Departament de Química Inorganica, Facultat de Químiques, Universitat de Barcelona, Diagonal 647, Barcelona 08028, Spain.
(2) Postdoctoral Research Associate, 1989–1990. Present address: Enitricerche, 20097 S. Donato Milanese, Milan, Italy.
(3) Ojima, I.; Okabe, M.; Kato, K.; Kwon, H. B.; Horváth, I. T. *J. Am. Chem. Soc.* **1988**, *110*, 150.
(4) (a) Horváth, I. T.; Bor, G.; Garland, M.; Pino, P. *Organometallics* **1986**, *5*, 1441. (b) Bor, G. *Pure Appl. Chem.* **1986**, *58*, 543.
(5) Spindler, F.; Bor, G.; Dietler, U. K.; Pino, P. *J. Organomet. Chem.* **1981**, *213*, 303.
(6) Horváth, I. T. *Organometallics* **1986**, *5*, 2333.
(7) Bojczuk, M.; Heaton, B. T.; Johnson, S.; Ghilardi, C. A.; Orlandini, A. *J. Organomet. Chem.* **1988**, *341*, 473.
(8) Bahsoun, A. A.; Osborn, J. A.; Voelker, C.; Bonet, J. J.; Lavigne, G. *Organometallics* **1982**, *1*, 1114.
(9) Eshtiagh-Hosseini, H.; Nixon, J. F. *J. Organomet. Chem.* **1978**, *150*, 129.
(10) Labroue, D.; Queau, R.; Poilblanc, R. *J. Organomet. Chem.* **1980**, *186*, 101.
(11) Horváth, I. T.; Zsolnai, L.; Huttner, G. *Organometallics* **1986**, *5*, 180.
(12) Horváth, I. T. *Polyhedron* **1988**, *7*, 2345.
(13) Hughes, R. P. In *Comprehensive Organometallic Chemistry*; Wilkinson, G., Stone, F. G. A., Abel, E., Eds.; Pergamon Press: Elmsford, NY, 1982; Vol. 5, Chapter 35, and references cited therein.

0276-7333/91/2310-3211$02.50/0

tert-butyl isocyanide (CN-Bu^t), cyclohexyl isocyanide (CN-Cy), and 2,6-dimethylphenyl isocyanide (CN-DMP-2,6).

The reaction of $Co_2Rh_2(CO)_{12}$ with excess amounts of CN-Bu^t in *n*-hexane at room temperature was accompanied by a gradual change in the color of the solution from reddish brown to dark orange, which indicates the formation of a dinuclear complex. This color change was faster under CO than under N_2, which is consistent with the dinuclear complex formation.

When 2 equiv of CN-Bu^t were used, an orange complex (**1a**) was obtained as a liquid. The close resemblance of the IR spectrum of **1a** to those reported for $CoRh(CO)_6(PEt_3)$ and $CoRh(CO)_6(MeCN)$[6] strongly suggests that **1a** is a monosubstituted dinuclear complex, $CoRh(CO)_6$(CN-Bu^t), in which the substitution has taken place on the rhodium; viz., the complex **1a** consists of a $Rh(CO)_2$(CN-Bu^t) fragment coupled with a $Co(CO)_4$ fragment through a Co–Rh bond and two semibridging carbonyls (1956 m, 1933 vs cm^{-1}) (eq 1). As has been pointed out for the

$$Co_2Rh_2(CO)_{12} + 2CN\text{-}Bu^t \rightarrow \underset{\mathbf{1a}}{2(CO)_4CoRh(CO)_2(CN\text{-}Bu^t)} \quad (1)$$

related triethylphosphine complexes,[6,14] $CoRh(CO)_{7-n}(PEt)_n$ (n = 1, 2), **1a** should be coordinatively unsaturated and possesses a polar metal–metal bond.

When 4 equiv of CN-Bu^t were allowed to react with $Co_2Rh_2(CO)_{12}$ at room temperature, another complex (**2a**) was obtained as an orange-red solid. The IR spectrum of the *n*-hexane solution of **2a** shows a pattern similar to that of **1** with all the bands shifted to lower frequencies, which closely resembles that of $CoRh(CO)_5(PEt_3)_2$.[6] This fact indicates that the second substitution takes place without changing the overall geometry of the complex; i.e., one more carbonyl ligand is substituted by CN-Bu^t at the Rh center to give $CoRh(CO)_5$(CN-Bu^t)$_2$ (**2a**). The ^{1}H NMR spectrum of **2a** in $CDCl_3$ shows two singlets ascribed to Bu^t protons at δ 1.47 and 1.49 in ca. 1:1 ratio, which indicates the existence of cis and trans isomers.

$$Co_2Rh_2(CO)_{12} + 4CN\text{-}Bu^t \rightarrow \underset{\mathbf{2a}}{2(CO)_4CoRh(CO)(CN\text{-}Bu^t)_2} + 2CO \quad (2)$$

Both complexes, **1a** and **2a**, are air-sensitive, unstable under vacuum, and soluble in *n*-hexane, giving orange solutions. Unfortunately, further characterization of those complexes has not been successful because of their instability during isolation procedures.

The reaction of $Co_2Rh_2(CO)_{12}$ with 8 equiv of CN-Bu^t in *n*-hexane gave a yellow precipitate. The IR spectrum of the precipitate in dichloromethane shows only two bands at 2166 and 1888 cm^{-1}. The band at high frequency corresponds to the CN stretching and the band at 1888 cm^{-1} is characteristic of the tetracarbonylcobalt anion, $[Co(CO)_4]^-$. Based on the IR spectrum and the elemental analysis, this product was identified as $[Rh(CN\text{-}Bu^t)_4][Co(CO)_4]$ (**3a**) (eq 3). The result clearly indicates that

$$Co_2Rh_2(CO)_{12} + 8CN\text{-}R \rightarrow 2[Rh(CN\text{-}R)_4][Co(CO)_4] + 2CO \quad (3)$$

3a, R = Bu^t
3b, R = Cy
3c, R = 2,6-DMP

the addition of two more equivalents of CN-Bu^t gives an ionic complex by breaking the Co–Rh bond. When similar substitution reactions of $Co_2Rh_2(CO)_{12}$ were carried out with variable amounts of CN-Cy, only an ionic complex, $[Rh(CN\text{-}Cy)_4][Co(CO)_4]$ (**3b**), was isolated. In a similar manner, $[Rh(CN\text{-}DMP\text{-}2,6)_4][Co(CO)_4]$ (**3c**) was obtained as crystals. These complexes (**3a–c**) are the first examples of tetrakis(isocyanide)rhodium complexes with a transition-metal carbonyl species as the counteranion.

Attempted synthesis of tris(isocyanide) complex $CoRh(CO)_4(CN\text{-}Bu^t)_3$, using 6 equiv of CN-Bu^t, was unsuccessful; viz., the products of the reactions were **2a** and **3a** (eq 4).

$$Co_2Rh_2(CO)_{12} + 6CN\text{-}Bu^t \rightarrow \underset{\mathbf{2a}}{CoRh(CO)_5(CN\text{-}Bu^t)_2} + \underset{\mathbf{3a}}{[Rh(CN\text{-}Bu^t)_4][Co(CO)_4]} \quad (4)$$

Complexes **3a–c**, especially **3c**, exhibit a peculiar behavior in solution. Complex **3a** precipitates as a yellow solid from *n*-hexane and its solution is yellow in dichloromethane or chloroform, but it becomes a reddish pink solid on evaporation of the solvent. Complex **3c** precipitates as orange-red crystals, but its solution in dichloromethane or chloroform is yellow. Complex **3b** precipitates as a blue solid from *n*-hexane but its solutions in benzene, dichloromethane, and chloroform are yellow. Removal of the solvents from these solutions gives a reddish pink solid, which, very slowly, is converted to the blue form under nitrogen.

It is known that cationic, homoleptic isocyanide complexes of rhodium, $[Rh(CN\text{-}R)_4]^+X^-$ (X = halide, BF_4, BPh_4, or PF_6), exhibit unusual behavior in solution; viz., the color of the solution is dependent upon the counterion and the concentration.[13] It has been shown that the discrete $[Rh(CN\text{-}R)_4]$ cations have a square-planar geometry and can form oligomeric species of the type $[Rh_n(CN\text{-}R)_{4n}]^{n+}$ by face to face stacking of the planar Rh(I) units in solution with formation of Rh–Rh bonds.[13] Accordingly, it is reasonable to assume that the ionic complexes **3a–c** consist of an anion, $[Co(CO)_4]^-$, with a tetrahedral geometry, and a cation, $[Rh(CN\text{-}R)_4]^+$, with a square-planar geometry.

The structure of **3c** was confirmed by single-crystal X-ray analysis. Summary of the data collection is listed in Table I. Selected bond distances, angles, and fractional coordinates of non-hydrogen atoms are summarized in Tables II, III, and IV, respectively. An ORTEP drawing of the molecular structure of **3a** with numbering is shown in Figure 1. The arrangement of molecules in a unit cell is depicted in Figure 2.

The $[Rh(CN\text{-}DMP\text{-}2,6)_4]$ moiety is slightly distorted square planar (∠C19–Rh1–C21, 171.1 (2)°; ∠C22–Rh1–C20, 166.7 (2)°) with three 2,6-dimethylphenyl groups in the plane and one almost perpendicular to the plane (<C20–N4–C31, 169.1 (4)°). The Rh–Co distance is 3.3785 (9) Å, which may suggest the existence of an attractive ionic interaction between the two metals. The $[Co(CO)_4]$ moiety is slightly distorted tetrahedral (∠C37–Co1–C39, 104.7 (2)°; ∠C39–Co1–C40, 118.8 (2)°) and one of the Co–CO bonds (Co1–C40–O3) is eclipsed with one of the Rh–CN–R bonds (Rh1–C20–N4). It should be noted that two of the carbonyls are slightly bent (∠Co1–C39–O2, 175.2 (4)°; ∠Co1–C40–O3, 173.3 (5)°) and the bond length of Co1–C37 (1.741 (6) Å) is slightly shorter than those of the other three (1.757 (5)–1.765 (5) Å). The C40–Rh1 distance (3.236 (5) Å) is considerably shorter than those of other two (3.365 (5) and 3.537 (4) Å). The observed distortion in both the rhodium and the cobalt moieties can be attributed to the steric constraint in crystalline state, particularly for the eclipsed Rh–CN–R bond and Co–CO bond.

(14) (a) Roberts, D. A.; Mercer, W. C.; Mahurak, S. M.; Geoffroy, G. L.; DeBrosse, C. W.; Cass, M. E.; Pierpont, C. G. *J. Am. Chem. Soc.* **1982**, *104*, 910. (b) Roberts, D. A.; Mercer, W. C.; Geoffroy, G. L.; Pierpont, C. G. *Inorg. Chem.* **1986**, *25*, 1439.

Table I. Summary of Crystallographic Data

	3a	6
empirical formula	$CoRhC_{40}H_{36}H_4O_4$	$Co_2Rh_2C_{33}H_{25}O_9P$
fw	798.59	920.21
cryst syst	monoclinic	triclinic
lattice params		
a, Å	10.820 (2)	10.389 (5)
b, Å	16.3206 (9)	17.40 (2)
c, Å	21.646 (4)	10.03 (2)
α, deg		105.9 (1)
β, deg	90.700 (7)	103.7 (1)
τ, deg		82.59 (6)
vol, Å^3	3822 (1)	1690 (7)
space group	$P2_1/c$ (No. 14)	$P\bar{1}$ (No. 2)
Z value	4	2
d_{calc}, g/cm^3	1.39	1.81
$F(000)$	1632	908
abs coeff μ, cm^{-1}	9.00 cm^{-1}	20.34 cm^{-1}
diffractometer	Enraf-Nonius CAD4	Enraf-Nonius CAD4
radiatn	Mo K_α (λ = 0.71069 Å) graphite monochromated	Mo K_α (λ = 0.71069 Å) graphite monochromated
temp, °C	23	23
$2\theta_{max}$, deg	49.9	53.9
no. observations ($I > 3\sigma(I)$)	3892	4832
no. of variables	451	428
residuals		
R^a	0.032	0.051
$R_w{}^a$	0.039	0.063
goodness of fit indicator	1.52	1.73
max shift in final cycle	0.04	0.19
largest peak in final diff map, e$^-$/Å^3	0.40	1.23

$^a R = \sum||F_o| - |F_c||/\sum|F_o|$; $R_w = [\sum_w(|F_o| - |F_c|)^2/\sum_w F_o^2]^2$.

Table II. Selected Bond Distances for [Rh(CN-DMP-2,6)$_4$][Co(CO)$_4$] (3c)

A–B	dist, Å	A–B	dist, Å
Rh1–Co1	3.3785 (9)	C19–N1	1.158 (5)
Rh1–C19	1.945 (4)	C20–N4	1.159 (5)
Rh1–C20	1.943 (5)	C21–N3	1.147 (5)
Rh1–C21	1.963 (4)	C22–N2	1.146 (5)
Rh1–C22	1.960 (4)	N1–C13	1.403 (5)
Rh1–C38	3.537 (4)	N2–C7	1.415 (5)
Rh1–C39	3.365 (5)	N3–C1	1.409 (5)
Rh1–C40	3.236 (5)	N4–C31	1.396 (5)
Co1–C37	1.741 (6)	O1–C38	1.144 (5)
Co1–C38	1.757 (5)	O2–C39	1.148 (5)
Co1–C39	1.765 (5)	O3–C40	1.151 (5)
Co1–C40	1.761 (5)	O4–C37	1.166 (6)

As Figure 2 shows, the cationic rhodium moieties do not form dimeric or oligomeric complexes making a Rh–Rh bond, which is known[13] for usual $[Rh(CN\text{-}R)_4]^+X^-$-type homoleptic isocyanide complexes in which the counteranion, X^-, is halide, $^-BF_4$, $^-BPh_4$, or $^-PF_6$. It is possible to discuss that these new Rh–Co mixed-metal isocyanide complexes (3) keep the $[Co(CO)_4]$ moiety close to the rhodium moiety instead of forming $[Rh_n(CN\text{-}R)_{4n}]^{n+}$ species. However, the fact that the cyclohexyl isocyanide complex **3b** gives a blue solid whereas *tert*-butyl and 2,6-DMP isocyanide complexes **3a** and **3c**, respectively, do not form a blue solid, giving only reddish pink or orange-red solids, may strongly suggest that **3b** indeed forms a dimeric dicationic complex, whereas **3a** and **3c** cannot form such dimeric species because of the bulkiness of the substituents.

Table III. Selected Bond Angles for [Rh(CN-DMP-2,6)$_4$][Co(CO)$_4$] (3c)

A–B–C	angle, deg	A–B–C	angle, deg
C19–Rh1–C21	171.1 (2)	Co1–C38–O1	178.1 (4)
C19–Rh1–C20	88.2 (2)	Co1–C39–O2	175.2 (4)
C20–Rh1–C21	85.4 (2)	Co1–C40–O3	173.3 (5)
C21–Rh1–C22	93.0 (2)	Co1–C37–O4	179.3 (5)
C22–Rh1–C19	91.9 (2)	C19–N1–C13	171.0 (4)
C37–Co1–C38	109.0 (2)	C20–N4–C31	169.1 (4)
C37–Co1–C39	104.7 (2)	C21–N3–C1	174.1 (4)
C37–Co1–C40	102.6 (2)	C22–N2–C7	176.5 (4)
C38–Co1–C40	112.6 (2)	N1–C13–C14	118.3 (5)
C39–Co1–C40	118.8 (2)	N1–C13–C18	117.7 (4)
Rh1–C19–N1	175.2 (4)	N2–C7–C8	117.4 (4)
Rh1–C20–N4	174.4 (4)	N2–C7–C12	117.5 (4)
Rh1–C21–N3	174.0 (4)	N3–C1–C2	118.3 (4)
Rh1–C22–N3	178.4 (4)	N4–C1–C6	117.8 (4)

Table IV. Positional Parameters and B(eq) Values (Å^2) for [Rh(CN-DMP-2,6)$_4$][Co(CO)$_4$] (3c)

atom	x	y	z	B(eq)
Rh1	0.24685 (3)	0.13554 (2)	0.13011 (2)	4.89 (2)
Co1	0.17325 (5)	0.13540 (4)	0.28134 (3)	5.45 (3)
O1	0.4179 (3)	0.0633 (2)	0.2904 (2)	7.5 (2)
O2	0.0100 (3)	0.0127 (2)	0.2269 (2)	7.7 (2)
O3	0.1731 (4)	0.3051 (2)	0.2405 (2)	8.8 (2)
O4	0.0764 (4)	0.1560 (3)	0.4051 (2)	10.0 (3)
N1	-0.0150 (3)	0.1013 (2)	0.0764 (2)	5.4 (2)
N2	0.3076 (3)	-0.0490 (2)	0.1481 (2)	5.4 (2)
N3	0.5119 (3)	0.1965 (2)	0.1622 (2)	5.2 (2)
N4	0.2226 (3)	0.3120 (2)	0.0786 (2)	5.6 (2)
C1	0.6239 (4)	0.2376 (3)	0.1750 (2)	5.0 (2)
C2	0.6268 (4)	0.3219 (3)	0.1688 (2)	5.5 (2)
C3	0.7377 (5)	0.3607 (3)	0.1820 (2)	6.5 (3)
C4	0.8382 (5)	0.3166 (4)	0.1999 (2)	7.2 (3)
C5	0.8340 (4)	0.2324 (4)	0.2060 (2)	6.8 (3)
C6	0.7241 (4)	0.1911 (3)	0.1938 (2)	5.7 (3)
C7	0.3329 (4)	-0.1339 (3)	0.1516 (2)	5.4 (2)
C8	0.4549 (5)	-0.1574 (3)	0.1633 (2)	6.2 (3)
C9	0.4770 (5)	-0.2410 (3)	0.1647 (2)	7.3 (3)
C10	0.3824 (7)	-0.2960 (3)	0.1545 (3)	8.1 (3)
C11	0.2634 (5)	-0.2702 (3)	0.1440 (2)	7.2 (3)
C12	0.2355 (5)	-0.1871 (3)	0.1421 (2)	5.7 (2)
C13	-0.1358 (4)	0.1034 (3)	0.0521 (2)	5.4 (2)
C14	-0.2002 (4)	0.0305 (4)	0.0472 (2)	6.7 (3)
C15	-0.3217 (5)	0.0358 (5)	0.0240 (3)	9.3 (4)
C16	-0.3703 (6)	0.1088 (7)	0.0075 (3)	10.8 (5)
C17	-0.3040 (5)	0.1787 (5)	0.0118 (3)	8.6 (4)
C18	-0.1822 (4)	0.1779 (4)	0.0338 (2)	6.5 (3)
C19	0.0829 (4)	0.1106 (2)	0.0974 (2)	5.0 (2)
C20	0.2259 (4)	0.2465 (3)	0.0993 (2)	5.6 (2)
C21	0.4163 (4)	0.1697 (2)	0.1510 (2)	4.9 (2)
C22	0.2846 (3)	0.0192 (3)	0.1423 (2)	4.6 (2)
C23	0.5153 (5)	0.3691 (3)	0.1488 (3)	7.5 (3)
C24	0.7138 (4)	0.1008 (4)	0.2017 (2)	7.2 (3)
C25	0.5540 (5)	-0.0957 (4)	0.1737 (3)	8.3 (3)
C26	0.1081 (5)	-0.1574 (3)	0.1302 (3)	7.9 (3)
C27	-0.1065 (5)	0.2538 (4)	0.0366 (2)	8.3 (3)
C28	-0.1463 (5)	-0.0490 (4)	0.0673 (3)	8.8 (4)
C29	0.0865 (7)	0.4500 (4)	0.1196 (3)	11.7 (4)
C30	0.3834 (6)	0.3105 (4)	-0.0228 (3)	10.8 (4)
C31	0.2379 (4)	0.3860 (2)	0.0472 (2)	4.9 (2)
C32	0.1742 (5)	0.4542 (3)	0.0665 (2)	7.1 (3)
C33	0.1936 (7)	0.5257 (3)	0.0348 (3)	9.9 (4)
C34	0.2715 (7)	0.5287 (4)	-0.0128 (3)	9.9 (4)
C35	0.3350 (6)	0.4603 (4)	-0.0317 (3)	9.0 (4)
C36	0.3165 (5)	0.3862 (3)	-0.0020 (2)	6.3 (3)
C37	0.1159 (4)	0.1475 (3)	0.3556 (3)	6.9 (3)
C38	0.3222 (4)	0.0928 (3)	0.2863 (2)	5.3 (2)
C39	0.0739 (4)	0.0630 (3)	0.2461 (2)	5.8 (2)
C40	0.1739 (4)	0.2365 (3)	0.2530 (2)	6.2 (3)

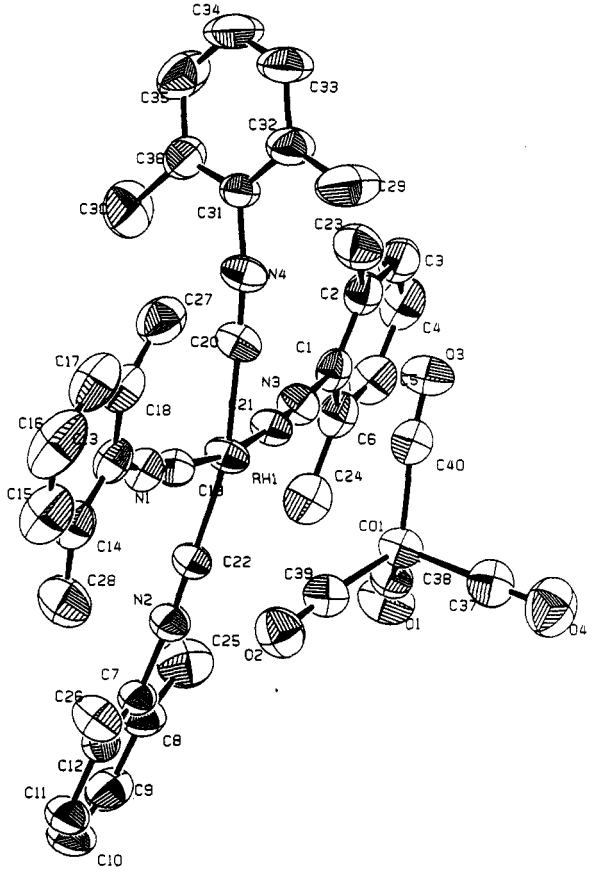

Figure 1. ORTEP drawing of $[Rh(CN\text{-}DMP\text{-}2,6)_4][Co(CO)_4]$ (**3c**).

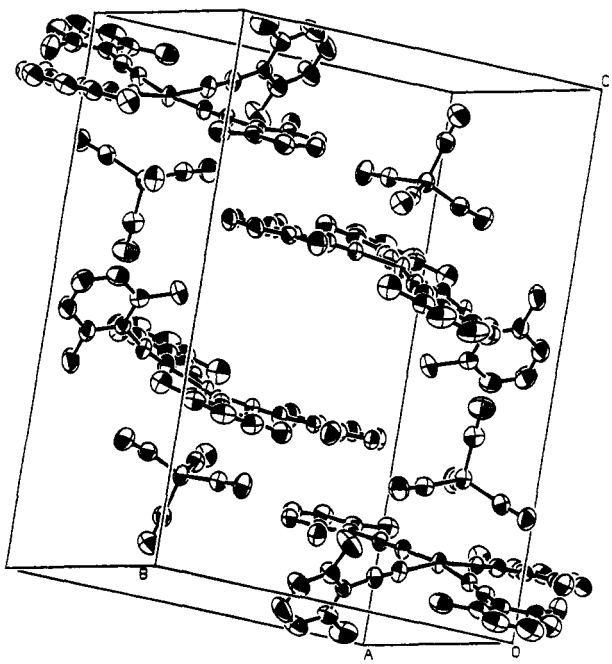

Figure 2. Arrangement of **3c** molecules in a unit cell.

No phosphine counterparts for compounds **2** and **3** have been reported in the literature. This fact may be ascribed to the characteristics of the isocyanide ligands, which have much smaller cone angles than the phosphine ligands.

It is known that isocyanide ligands stabilize +1 and +2 oxidation states better than the zero oxidation state, in general, and substitution of CO by CN-R leads to an increase in stability.[13] Indeed, the results for **2** and **3** follow this generalization, viz., the C≡N stretching frequencies in their IR spectra are in all cases higher than that of the free ligand, which is in agreement with the polarity of the Co–Rh bond in this type of mixed-metal complex (vide supra); i.e., the isocyanide ligands serve as pure donor ligands in these complexes, and all the complexes obtained are stable at room temperature.

Reactions with Alkynes. It has been shown that tetranuclear clusters are prone to open their cluster framework to give a butterfly structure in the presence of alkynes.[14] It has also been reported that $Co_2Rh_2(CO)_{12}$ reacts with bis(pentafluorophenyl)acetylene to give a mixed-metal butterfly complex, $Co_2Rh_2(CO)_{10}(C_6F_5C{\equiv}CC_6F_5$ (**4a**), in which the acetylene inserts into the Co–Co bond.[11] In order to further investigate the selective cleavage of the metal–metal bonds in this mixed-metal cluster, $Co_2Rh_2(CO)_{12}$, in the reactions with 1-alkynes as well as the nature of the acetylenic methine moiety in the Co–Rh mixed-metal butterfly clusters, we carried out the reactions of $Co_2Rh_2(CO)_{12}$ with 1-hexyne, phenylacetylene, and trimethylsilylacetylene.

When an alkyne was added to a solution of $Co_2Rh_2(CO)_{12}$ in *n*-hexane at room temperature, the color of the solution gradually changed from reddish brown to deep purple. An IR spectrum of the reaction mixture showed a completely new pattern in the carbonyl region, indicating the formation of an alkyne-bridged butterfly cluster, $Co_2Rh_2(CO)_{10}(HC{\equiv}CR)$ (**5a**, R = Bu^n; **5b**, R = Ph; **5c**, R = $SiMe_3$) (eq 5). New mixed-metal butterfly complexes

$$Co_2Rh_2(CO)_{12} + HC{\equiv}CR \rightarrow Co_2Rh_2(CO)_{10}(HC{\equiv}CR) + 2CO \quad (5)$$

5a, R = Bu^n
5b, R = Ph
5c, R = $SiMe_3$

(**5a–c**) were isolated from the reaction mixture through column chromatography on silica gel (for **5a,b**) or by recrystallization from *n*-hexane (for **5c**) in nearly quantitative yields.

The IR spectra of **5a–c** resemble each other in spite of the fact that these clusters incorporate quite different 1-alkynes. The observed shift of the carbonyl stretching bands to lower frequencies from those values reported for the bis(pentafluorophenyl)acetylene complex **4a**[11] can be ascribed to the stronger donor ability of the 1-alkyne ligands used in comparison with electron-deficient bis(pentafluorophenyl)acetylene. An open tetranuclear butterfly structure has a 2-fold axis that interchanges the wingtip and the hinge positions between themselves. Accordingly, if an unsymmetrical alkyne such as 1-alkyne is used to *close* the structure, this symmetry should be destroyed. Indeed, such lowering of symmetry is obvious for **5c**, whose IR spectrum shows more bands in the carbonyl region than the authentically prepared diphenylacetylene complex, $Co_2Rh_2(CO)_{10}(PhC{\equiv}CPh)$ (**4b**),[11] as well as **5a** and **5b**. This may be due to the bulkiness of the trimethylsilyl group, which would considerably distort the butterfly structure, whereas the distortion caused by *n*-butyl and phenyl groups may well be too small to be clearly observed.

The NMR spectra of **5a–c** are also consistent with the 1-alkyne-bridged butterfly structure. The ^1H NMR spectra of **5a**, **5b**, and **5c** show singlets at δ 8.85, 8.95, and 9.32 ppm, respectively, corresponding to the acetylenic hydrogens. This remarkable downfield shift of the acetylenic hydrogen is characteristic of the hydrogen atoms bound to carbons interacting either σ or π with metals.[15] In the ^1H NMR

(15) (a) Sappa, E.; Tiripicchio, A.; Braunstein, P. *Chem. Rev.* **1983**, *83*, 203. (b) Raithby, P. R.; Rosales, M. J. *Adv. Inorg. Chem. Radiochem.* **1985**, *29*, 169.

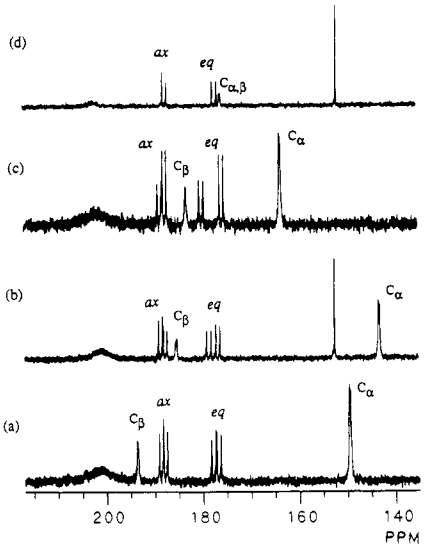

Figure 3. Carbonyl region of the ^{13}C NMR spectra of $Co_2Rh_2(CO)_{10}(RC{\equiv}CR')$. ($RC{\equiv}CR'$: **5a**, $HC{\equiv}CBu^n$; **5b**, $HC{\equiv}CPh$; **5c**, $HC{\equiv}CSiMe_3$; **4b**, $PhC{\equiv}CPh$.

of **5a**, considerable lower field shift of the resonance due to the methylene group adjacent to the triple bond is observed, which appears at δ 2.75 ppm. The fact strongly indicates the closed butterfly structure as well.

The carbonyl region of the ^{13}C NMR spectra of **5a–c** and **4b** taken at 25 °C are depicted in Figure 3. As Figure 3 shows, the two acetylenic carbons, $C_\alpha(\equiv CH)$ and $C_\beta(\equiv CR)$, appear at δ 143–164 ppm and δ 183–194 ppm, respectively. The higher field peak of the two is assigned to C_α on the basis of their peak height; i.e., C_α is a higher peak than C_β probably due to shorter T_1 and also by comparison of the chemical shifts with that of the C_α (C_β) carbon (175.8 ppm) of the diphenylacetylene complex (**4b**). Both peaks are multiplets, indicating their bonding to both rhodium atoms. Consistent with the ^1H NMR results, the chemical shift of C_α of **5a** (193.5 ppm) is larger than those of **5b** (185.2 ppm) and **5c** (183.2 ppm). This remarkable lower field shift of C_α and C_β should be attributed to the carbon atoms σ–π-bonded to metals, which are partially carbenic in character.[15] It has been shown that these resonances move to lower field as the number of metals interacting with the acetylenic ligand increases.[15]

For the carbonyl carbon atoms, complexes **5a–c** show two sets of two doublets (δ 175–180 and 187–189 ppm) in which each doublet corresponds to one carbonyl and a very broad peak (δ 201 ppm) corresponding to six carbonyl ligands. By analogy with the assignment reported for **4b**,[11] the broad signal centered at δ 201 ppm is assigned to the terminal, bridging, and semibridging carbonyl ligands bonded to the cobalt atoms, which are exchanging evenly at room temperature. The four carbonyl ligands bonded to the rhodium atoms are rigid at 25 °C and give rise to four doublets. The set of resonances at lower field (δ 175–180 ppm; J_{Rh-C} = 60 and 61 Hz for **5a**, 60 and 60 Hz for **5b**, 61 and 62 Hz for **5c**) are assigned to axial carbonyl ligands and those at higher field (δ 187–189 ppm; J_{Rh-C} = 67 and 70 Hz for **5a**, 66 and 68 Hz for **5b**, 66 and 67 Hz for **5c**) to equatorial carbonyl ligands on the basis of the results on the selective substitution of the equatorial carbonyl ligands by triphenylphosphine (vide infra). The other peak present in the spectrum of **5b** (152.4 ppm) as well as that of **4b** (151.7 ppm) is assigned to the ipso carbon (C_1) of the phenyl ring.

In order to further investigate the reactivity of the 1-alkyne-bridged Co–Rh mixed-metal butterfly complexes,

Table V. Selected Bond Distances for $Co_2Rh_2(CO)_9(\mu_4,\eta^2\text{-}HC{\equiv}CBu^n)(PPh_3)$ (6)

A–B	dist, Å	A–B	dist, Å
Rh1–Rh2	2.700 (4)	Rh1–Co1	2.590 (4)
Rh1–Co2	2.569 (2)	Rh1–C2	2.153 (8)
Rh1–C7	1.91 (1)	Rh1–C8	1.93 (1)
Rh1–C10	2.099 (7)	Rh2–Co1	2.606 (3)
Rh2–Co2	2.555 (4)	Rh2–P1	2.339 (4)
Rh2–C4	2.066 (8)	Rh2–C9	1.880 (8)
Rh2–C15	2.147 (8)	Co1–C1	1.77 (1)
Co1–C2	1.857 (8)	Co1–C3	1.79 (1)
Co1–C10	2.053 (7)	Co1–C15	2.100 (7)
Co2–C4	1.886 (9)	Co2–C5	1.771 (9)
Co2–C6	1.742 (9)	Co2–C10	2.175 (7)
Co2–C15	2.051 (8)	P1–C21	1.816 (8)
P1–C31	1.814 (9)	P1–C41	1.819 (8)
O1–C1	1.12 (1)	O2–C2	1.16 (1)
O3–C3	1.15 (1)	O4–C4	1.15 (1)
O5–C5	1.15 (1)	O6–C6	1.15 (1)
O7–C7	1.15 (1)	O8–C8	1.12 (1)
O9–C9	1.15 (1)	C10–C15	1.43 (1)

Table VI. Selected Bond Angles for $Co_2Rh_2(CO)_9(\mu_4,\eta^2\text{-}HC{\equiv}CBu^n)(PPh_3)$ (6)

A–B–C	angle, deg	A–B–C	angle, deg
Rh2–Rh1–Co1	59.0 (1)	Rh2–Rh1–Co2	58.0 (1)
Co1–Rh1–Co2	89.2 (1)	Rh1–Rh2–Co1	58.4 (1)
Rh1–Rh2–Co2	58.5 (1)	Co1–Rh2–Co2	89.1 (1)
Rh1–Co1–Rh2	62.6 (1)	Rh1–Co2–Rh2	63.6 (1)
C10–Co2–C15	39.3 (3)	C10–Co1–C15	40.2 (3)
Rh1–C10–C15	106.1 (5)	C11–C10–C15	126.0 (7)
Rh2–C15–C10	108.6 (5)	C10–C15–H25	121 (6)
Rh2–P1–C21	114.5 (3)	Rh2–P1–C31	114.6 (3)
Rh2–P1–C41	115.4 (3)	Rh1–Rh2–P1	173.18 (6)
Co1–C1–O1	173.6 (9)	Rh1–C2–O2	133.5 (7)
Co1–C2–O2	146.4 (7)	Co1–C3–O3	177.5 (8)
Rh2–C4–O4	138.0 (6)	Co2–C4–O4	141.3 (6)
Co2–C5–O5	177 (1)	Co2–C6–O6	172.8 (8)
Rh1–C7–O7	178.5 (8)	Rh1–C8–O8	175.9 (9)
Rh2–C9–O9	175.8 (7)		

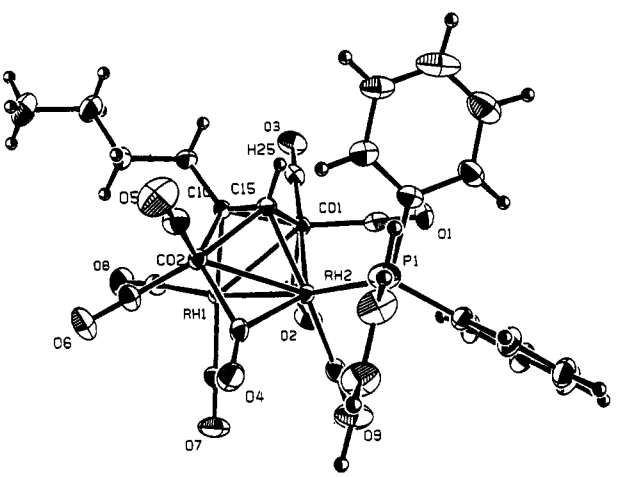

Figure 4. ORTEP drawing of $Co_2Rh_2(CO)_{10}(HC{\equiv}CBu^n)(PPh_3)$ (**6**).

we carried out the substitution reaction of **5a** with triphenylphosphine.

The reaction of **5a** with 1 equiv of triphenylphosphine in *n*-hexane (or dichloromethane) resulted in the formation of the corresponding monosubstituted cluster $Co_2Rh_2(CO)_9(HC{\equiv}CBu^n)(PPh_3)$ (**6a**) as the predominant product. As the minor product, a disubstituted cluster, $Co_2Rh_2(CO)_8(HC{\equiv}CBu^n)(PPh_3)_2$ (**7a**), was obtained. It should be noted that in both cases only a single isomer among the possible regio- and stereoisomers was formed; i.e., the substitution reaction is extremely regio- and stereoselective. Complex **7a** was obtained in almost quantitative yield

Table VII. Positional Parameters and B(eq) Values (Å²) for $Co_2Rh_2(CO)_9(\mu_4,\eta^2\text{-HCCBu}^n)(PPh_3)$ (6)

atom	x	y	z	B(eq)
Rh1	0.05665 (6)	-0.36688 (3)	-0.11793 (6)	2.32 (2)
Rh2	0.17868 (6)	-0.24482 (3)	0.08182 (6)	2.16 (2)
Co1	0.2188 (1)	-0.39141 (6)	0.1083 (1)	2.51 (4)
Co2	0.2364 (1)	-0.29441 (6)	-0.1628 (1)	2.55 (4)
P1	0.3082 (2)	-0.1481 (1)	0.2516 (2)	2.53 (7)
O1	0.2956 (8)	-0.3243 (4)	0.4097 (6)	5.6 (3)
O2	-0.0564 (6)	-0.3927 (5)	0.1218 (7)	5.2 (3)
O3	0.3020 (7)	-0.5562 (4)	0.1289 (8)	5.1 (3)
O4	0.0967 (8)	-0.1387 (4)	-0.1214 (7)	5.8 (3)
O5	0.4504 (8)	-0.2342 (5)	-0.240 (1)	7.3 (4)
O6	0.0559 (8)	-0.3187 (5)	-0.4362 (7)	5.7 (3)
O7	-0.2144 (7)	-0.2733 (4)	-0.1569 (8)	6.0 (3)
O8	-0.0434 (8)	-0.5135 (4)	-0.3502 (7)	5.6 (3)
O9	-0.0759 (6)	-0.1614 (4)	0.1628 (7)	4.9 (3)
C1	0.2645 (9)	-0.3461 (5)	0.292 (1)	3.8 (4)
C2	0.0350 (8)	-0.3886 (5)	0.0766 (8)	3.3 (3)
C3	0.2668 (8)	-0.4924 (5)	0.1191 (8)	3.2 (3)
C4	0.1493 (9)	-0.1953 (5)	-0.0890 (7)	3.3 (3)
C5	0.369 (1)	-0.2585 (5)	-0.206 (1)	3.9 (4)
C6	0.124 (1)	-0.3126 (5)	-0.3253 (8)	3.5 (3)
C7	-0.1130 (9)	-0.3092 (5)	-0.1414 (9)	3.3 (3)
C8	-0.0022 (9)	-0.4610 (5)	-0.2634 (9)	3.4 (3)
C9	0.0229 (8)	-0.1923 (5)	0.1375 (8)	3.1 (3)
C10	0.2602 (7)	-0.4021 (4)	-0.0865 (7)	2.3 (3)
C11	0.3268 (8)	-0.4797 (5)	-0.1591 (8)	3.2 (3)
C12	0.323 (1)	-0.4900 (5)	-0.3149 (8)	3.7 (3)
C13	0.390 (1)	-0.5685 (6)	-0.3791 (1)	5.1 (4)
C14	0.374 (1)	-0.5867 (8)	-0.537 (1)	7.4 (6)
C15	0.3260 (8)	-0.3357 (4)	0.0121 (7)	2.5 (3)
C21	0.3238 (8)	-0.0605 (5)	0.1928 (8)	3.0 (3)
C22	0.207 (1)	-0.0164 (5)	0.144 (1)	4.1 (4)
C23	0.214 (1)	0.0507 (6)	0.102 (1)	5.4 (5)
C24	0.334 (1)	0.0772 (6)	0.109 (1)	5.3 (5)
C25	0.446 (1)	0.0357 (6)	0.156 (1)	5.3 (5)
C26	0.441 (1)	-0.0323 (5)	0.196 (1)	4.0 (4)
C31	0.4791 (8)	-0.1828 (5)	0.3109 (9)	3.3 (3)
C32	0.557 (1)	-0.2148 (5)	0.213 (1)	3.8 (3)
C33	0.687 (1)	-0.2419 (6)	0.252 (1)	4.8 (4)
C34	0.742 (1)	-0.2374 (8)	0.392 (2)	6.9 (6)
C35	0.667 (1)	-0.2052 (7)	0.491 (1)	6.4 (6)
C36	0.536 (1)	-0.1774 (6)	0.453 (1)	4.2 (4)
C41	0.2445 (8)	-0.1021 (5)	0.4113 (8)	3.1 (3)
C42	0.268 (1)	-0.0234 (6)	0.486 (1)	4.2 (4)
C43	0.217 (1)	0.0115 (6)	0.606 (1)	4.6 (4)
C44	0.141 (1)	-0.0309 (6)	0.650 (1)	5.2 (5)
C45	0.115 (1)	-0.1084 (6)	0.578 (1)	4.9 (4)
C46	0.166 (1)	-0.1443 (5)	0.4572 (8)	3.8 (4)
H25	0.43 (1)	-0.339 (6)	0.05 (1)	6 (3)

by the reaction of **5a** with excess triphenylphosphine.

In a similar manner, $Co_2Rh_2(CO)_8(HC{\equiv}CPh)(PPh_3)_2$ (**6c**) and $Co_2Rh_2(CO)_9(HC{\equiv}CSiMe_3)(PPh_3)$ (**7b**) were synthesized.

The molecular structure of **6a** was determined by single-crystal X-ray analysis. Summary of the data collection is found in Table I. Selected bond distances and angles are listed in Tables V and VI, respectively, and fractional coordinates of non-hydrogen atoms are given in Table VII. An ORTEP drawing with numbering is shown in Figure 4.

The metal framework of **6a** has a butterfly structure with the cobalt atoms occupying the wingtip positions. The dihedral angle between the wings (Rh1–Rh2–Co1/Rh1–Rh2–Co2) is 110.85° and the nonbonding distance between the two cobalt atoms Co1 and Co2 is 3.621 (5) Å. The acetylene moiety is coordinated to the concave side such that the C–C bond is nearly parallel to the hinge of the butterfly. It coordinates to all metal atoms as a μ_4-η^2-ligand forming a distorted *closo*-$Co_2Rh_2C_2$ octahedron. Each cobalt atom is linked to two terminal carbonyls and there are two bridging carbonyl ligands along two opposite hinge-to-wingtip cobalt–rhodium bonds. The atoms Rh1 and Rh2 are bonded to two linear terminal carbonyl ligands and to one linear terminal carbonyl ligand, respectively. The Rh1 atom is bonded to C10 and Rh2 is bonded to C15 of the acetylenic moiety. The triphenylphosphine ligand is bonded to Rh2; viz., *triphenylphosphine has replaced an equatorial carbonyl at the less hindered side selectively.*

According to the well-known Dewar–Chatt–Duncanson model, the coordination of the acetylene can be formally described as the one consisting of two σ-bonds (C10–Rh1 and C15–Rh2) and a delocalized four-center π-bonding system between C10, Co1, C15, and Co2.

The spiro metallocycle Co1–C15–Co2–C10 is slightly distorted with two long (Co1–C15, 2.100 (7); Co2–C10, 2.175 (7) Å) and two short (Co1–C10, 2.053 (7); Co2–C15, 2.051 (8) Å) distances. The Rh2–C15 bond (2.147 (8) Å) is longer than the Rh1–C10 bond (2.099 (7) Å), and the acetylenic bond C10–C15 (1.43 (1) Å) has double-bond character. The observed C10–C15 bond distance for **6a** is considerably longer than the reported C–C distance for $Co_2Rh_2(CO)_{10}(F_5C_6C{\equiv}CC_6F_5)$ (1.369 (2) Å).[11] The lengthening of the C–C bond and the bending of the C–H and the C–Bu^n bonds away from the metal cluster (C10–C15–H25, 121 (6)°; C15–C10–C11, 126 (7)°) are the result of the coordination of the alkyne and can be taken as a measure of the decrease of the triple-bond character upon coordination. It is also a measure of the strength of the interaction between the butterfly cluster and alkyne, viz., the stronger the interaction with the cluster, the greater the possibility of finding long C–C distances. Consequently, it can be said that alkyne ligands bearing electron-releasing groups have stronger interactions with the butterfly clusters.

IR spectra of **6a** and **7a** show the expected shift of all the carbonyl stretching bands to lower frequencies from those for **5a**, as two carbonyl ligands are replaced, step by step, by two triphenylphosphine ligands; viz., triphenylphosphine is better donor ligand than CO, increasing the electron density on the metals in the clusters. For example, a consistent downfield shift of the broad peak corresponding to the rest of the carbonyl ligands that are exchanging at room temperature is observed from **5a** (201 ppm) to **6a** (207 ppm) and then to **7a** (215 ppm). This change in electron density is also reflected in their ^1H and ^{13}C NMR spectra. The ^1H NMR data for **5a**, **6a**, and **7a** are listed in Table VIII.

As Table VIII shows, the peaks corresponding to the *n*-butyl chain of the alkyne moiety shift to higher field

Table VIII. ^1H NMR Data for $Co_2Rh_2(CO)_{10}(HC{\equiv}CR)$ (5), $Co_2Rh_2(CO)_9(HC{\equiv}CR)(PPh_3)$ (6), and $Co_2Rh_2(CO)_8(HC{\equiv}CR)(PPh_3)_2$ (7) (a, R = Bu^n; b, R = Ph; c, R = $SiMe_3$)

	5a	5b	5c	6a	6c	7a	7b
$SiCH_3$			0.16 s		0.54 s		
CH_3	0.90 m			0.88 t		0.58 t	
CH_2CH_2	1.28 m			1.25 m		0.82 m, 1.01 m	
$\equiv CCH_2$	2.74 m			2.61 m		2.29 m	
PPh_3, Ph	7.44–7.66 m	7.10–7.25 m			6.68–7.75 m	7.47–7.69 m	6.75–7.75 m
≡CH	8.85 s	8.95 s	9.32	8.12 d (19.5)[a]	8.55 d (20.1)[a]	8.65 d (21.8)[a]	8.26 d (18.9)[a]

[a] J_{P-H} in hertz.

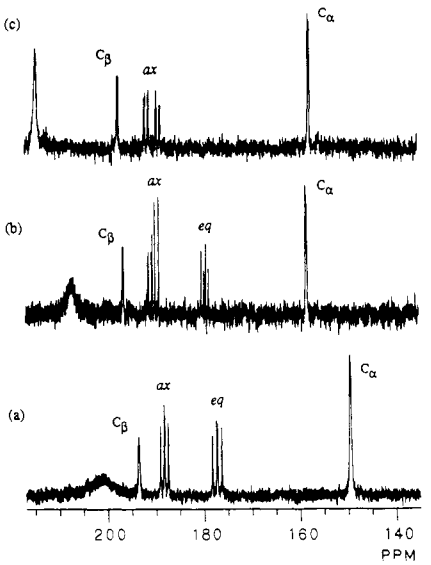

Figure 5. Carbonyl region of the ^{13}C NMR spectra of $Co_2Rh_2(CO)_{10-n}(HC{\equiv}CBu^n)(PPh_3)_n$: (a) **5a**, $n = 0$; (b) **6**, $n = 1$; (c) **7**, $n = 2$.

from **5a** to **6a** and then to **7a**, and the shift is much larger from **6a** to **7a** than from **5a** to **6a**. This upfield shift is due to the increase in electron density on the cluster as the carbonyl ligands are substituted by triphenylphosphine ligands. However, the larger upfield shift observed in the second substitution is most likely due to the fact that the second substitution occurs at the rhodium atom bonded to C_β, which bears an n-butyl group, while the first substitution takes place at the rhodium atom bonded to C_α, as confirmed by an X-ray analysis of **6a** (vide supra). Thus, the observed substantial upfield shift of *n*-butyl protons may well be due to the anisotropy of the phenyl group(s) of the triphenylphosphine on the C_β side.

The carbonyl region of the ^{13}C NMR spectra of **5a**, **6a**, and **7a** are depicted in Figure 5. As Figure 5 shows, there is a substantial downfield shift of C_α and C_β, especially C_α, for **6a** in comparison to **5a**, but the addition of another triphenylphosphine does not affect these resonances anymore. The peaks due to the carbonyl ligands bonded to the rhodiums are also affected by the substitution, but to a much lesser extent. It should be noted that the substitutions take place only with carbonyl ligands in the higher field, and the higher field carbonyls disappear in the spectrum of **7a**. Since the higher field carbonyls can be unambiguously assigned to the equatorial ones on the basis of the X-ray structure (Figure 3), it is concluded that the substitutions take place selectively with the equatorial carbonyls, first at Rh2 and then Rh1. In the spectrum of **6a**, the axial carbonyl of Rh1 appears as a doublet (J_{Rh-C} = 59.2 Hz) at δ 189.6 ppm while the axial carbonyl of Rh2 appear as doublets (J_{Rh-C} = 60.6 Hz; J_{P-C} = 12.0 Hz) at 191.1 ppm. An unusually large coupling between the phosphorus at Rh2 and the equatorial carbonyl at Rh1 is observed (δ 179.5 ppm; dd, J_{Rh-C} = 73 Hz; $^3J_{P-C}$ = 41 Hz). This unprecedented large three-bond coupling can be ascribed to the trans arrangement of the carbonyl and the phosphorus across the Rh–Rh bond.

As Table VIII shows, there is a substantial upfield shift of acetylenic hydrogen of C_α from **5a** (δ 8.85 ppm) to **6a** (δ 8.12 ppm), which is consistent with their ^{13}C NMR spectra. However, a considerable downfield shift of the acetylenic hydrogen is observed from **6a** to **7a** (8.65 ppm). This inconsistency can be attributed to the anisotropy of the phenyl groups of the triphenylphosphine at Rh2, viz., either the acetylenic hydrogen of C_α of **6a** is in the shielding zone of the phenyls or that of **7a** is in the deshielding zone of the phenyl group(s). The same discussion is applicable for **5b** versus **7b** and **5c** versus **6c** as shown in Table VIII.

Experimental Section

General Methods. Boiling points and melting points are uncorrected. ^1H and ^{13}C NMR spectra were recorded on a General Electric QE-300 spectrometer. Resonances are reported as shifts in parts per million downfield from tetramethylsilane and, unless otherwise noted, chloroform-d_1 was used as the solvent. IR spectra were recorded on a Perkin-Elmer 1600 FT-IR spectrophotometer with an HP 7470A plotter. Absorptions are designated in cm^{-1} relative to an internal laser standard. Spectra were measured by using a neat film or a solution of sample between NaCl plates or as Nujol mulls. Column chromatography was performed on MN-Kieselgel 60 (230–400 mesh) purchased from Brinkmann Instruments, Inc. Elemental analysis were performed by M-H-W Laboratories, Phoenix, AZ. All reactions were carried out under nitrogen or under carbon monoxide, and standard Schlenk and vacuum-line techniques were employed.

Materials. Solvents were refluxed over appropriate drying agents and distilled prior to use: *n*-hexane, pentane, heptane, benzene, and dichloromethane were distilled from calcium hydride; tetrahydrofuran and diethyl ether were distilled from sodium/benzophenone. The reagents, $RhCl_3{\cdot}3H_2O$ and $Co_2(CO)_8$, were obtained from Engelhard Industries KK and Strem Chemicals, Inc., respectively, and used as received. $NaCo(CO)_4$,[16] $Rh_2(CO)_4Cl_2$,[17] $Co_2Rh_2(CO)_{12}$,[18,4a] $Co_3Rh(CO)_{12}$,[18] and $Rh_4(CO)_{12}$[19] were prepared according to literature methods. The ligands, PPh_3, CN-Cy, CN-Bu^t, and CN-DMP-2,6 were obtained from Aldrich Chemical Co., Inc. The isocyanides were used as received and PPh_3 was recrystallized from hot methanol. All other chemicals were purchased from Aldrich Chemical Co., Inc.

Reactions with Isocyanides. Reactions of $Co_2Rh_2(CO)_{12}$ with 2 and 4 equiv of CN-Bu^t. The reaction was carried out under carbon monoxide atmosphere at room temperature. To a solution of $Co_2Rh_2(CO)_{12}$ (100 mg, 0.150 mmol) in 20 mL of *n*-hexane in a flask equipped with an addition funnel was added very slowly a solution of CN-Bu^t (25 mg, 0.30 mmol) in 10 mL of *n*-hexane, prepared under nitrogen. The mixture was stirred for 30 min at room temperature. During the stirring the brown color slowly changed to orange. Evaporation of the solvent in a flow of carbon monoxide gave $CoRh(CO)_6(CN\text{-}Bu^t)$ (**1a**) in quantitative yield as an orange liquid: IR (*n*-hexane, cm^{-1}) ν(CN) 2202 w, ν(CO) 2081 vs, 2041 vs, 2024 vs, 1982 s, 1956 m, 1933 vs. Because of the unstability of **1a** under vacuum, satisfactory elemental analyses have not been obtained. Nevertheless, we are quite sure about its structure on the basis of the fact that the formation of **1a** and its conversion to the disubstituted complex, $CoRh(CO)_5(CN\text{-}Bu^t)_2$ (**2a**) is readily monitored by FT-IR.

Next, to a solution of $Co_2Rh_2(CO)_{12}$ (66 mg, 0.10 mmol) in 20 mL of *n*-hexane at room temperature was added dropwise a solution of CN-Bu^t (33 mg, 0.40 mmol) in 10 mL of *n*-hexane under nitrogen. After the addition, the color immediately changed to orange. After the mixture was stirred for 30 min at room temperature, the solvent was reduced to a half of its volume and $CoRh(CO)_5(CN\text{-}Bu^t)_2$ (**2a**) precipitated in quantitative yield by cooling the solution to 0 °C. The orange-red precipitate was collected on a glass filter and dried under the flow of carbon monoxide and was immediately submitted to FT-IR and ^1H NMR measurements: IR (*n*-hexane, cm^{-1}) ν(CN) 2163 s; ν(CO) 2033 vw, 2005 vs, 1957 s, 1937 m, 1915 s. ^1H NMR ($CDCl_3$) δ 1.47 (s), 1.49 (s). Attempted recrystallization and chromatographic purification under carbon monoxide or nitrogen were hampered by decomposition.

Synthesis of $[Rh(CN\text{-}Bu^t)_4][Co(CO)_4]$ (3a). To a solution of $Co_2Rh_2(CO)_{12}$ (66 mg, 0.10 mmol) in 20 mL of *n*-hexane at room temperature was added dropwise a solution of CN-Bu^t (66 mg,

(16) Edgell, W. F.; Lyford, V. J. *Inorg. Chem.* **1970**, *9*, 1932.
(17) McCleverty, J. A.; Wilkinson, G. *Inorg. Synth.* **1966**, *8*, 211.
(18) Martinengo, S.; Chini, P.; Albano, V. G.; Cariati, F. *J. Organomet. Chem.* **1973**, *59*, 379.
(19) Martinengo, S.; Giordano, G.; Chini, P. *Inorg. Synth.* **1980**, *20*, 209.

0.80 mmol) in 10 mL of *n*-hexane under nitrogen. An orange precipitate formed immediately. The mixture was stirred for 1 h at room temperature. The orange precipitate was isolated by filtration and washed with *n*-hexane. Recrystallization from CH_2Cl_2/*n*-hexane afforded $[Rh(CN\text{-}Bu^t)_4][Co(CO)_4]$ (**3a**) in quantitative yield as a light yellow solid.

3a: Mp 149–151 °C. IR (CH_2Cl_2, cm^{-1}) ν(CN) 2166 vs; ν(CO) 1888 vs (br). IR (Nujol mull, cm^{-1}) ν(CN) 2169 vs; ν(CO) 1885 vs (br); ^1H NMR ($CDCl_3$) δ 1.53 (s). Anal. Calcd for $C_{24}H_{36}N_4O_4O_4CoRh$: C, 47.54; H, 5.98; N, 9.24. Found: C, 47.57; H, 6.02; N, 9.33.

Reaction of $Co_2Rh_2(CO)_{12}$ with 6 equiv of CN-Bu^t. To a solution of $Co_2Rh_2(CO)_{12}$ (66 mg, 0.10 mmol) in 80 mL of *n*-hexane in a flask equipped with an addition funnel was added dropwise a solution of CN-Bu^t (50 mg, 0.60 mmol) in 40 mL of *n*-hexane over a period of 1 h at room temperature under nitrogen. The color of the solution gradually changed from reddish brown to dark orange to light orange. When one-third of the isocyanide solution still remained in the addition funnel, a yellow precipitate began to form. After the addition was finished, the reaction mixture was stirred for an additional 30 min. Then the solvent was reduced to a half of its volume. Filtration of the reaction mixture gave a yellow precipitate and an orange solution. An IR of the yellow solid either in dichloromethane or as a Nujol mull identified it as $[Rh(CN\text{-}Bu^t)_4][Co(CO)_4]$ (**3a**) and an IR of the solution indicated the presence of $CoRh(CO)_5(CN\text{-}Bu^t)_2$ (**2a**).

Synthesis of $[Rh(CN\text{-}Cy)_4][Co(CO)_4]$ (3b). To a solution of $Co_2Rh_2(CO)_{12}$ (66 mg, 0.10 mmol) in 30 mL of *n*-pentane was added dropwise a solution of CN-Cy (87 mg, 0.80 mmol) in 10 mL of pentane with vigorous stirring. Initially a red precipitate was formed, but it redissolved quickly to form a dark red oil. The mixture was stirred for 2 h at room temperature, and then a blue precipitate was formed. The blue precipitate was isolated by filtration and washed with *n*-pentane to give $[Rh(CN\text{-}Cy)_4][Co(CO)_4]$ (**3b**) in quantitative yield. It is interesting to note that when **3b** was dissolved in benzene, chloroform, or dichloromethane, a yellow solution resulted, which yielded a reddish pink solid or film on evaporation of the solvent. Upon standing under nitrogen, the reddish pink solid was slowly converted to the blue solid.

Blue form: Mp 102 °C. IR (Nujol mull, cm^{-1}) ν(CN) 2207 m, 2167 vs; ν(CO) 1881 vs (br). ^1H NMR ($CDCl_3$) δ 1.50–2.50 (m, 40 H), 3.97 (br s, 4 H). Anal. Calcd for $C_{32}H_{44}N_4O_4CoRh$: C, 54.09; H, 6.24; N, 7.89. Found: C, 53.94; H, 6.28; N, 8.09.

Yellow form: IR (CH_2Cl_2, cm^{-1}) ν(CN) 2172 vs; ν(CO) 1888 vs (br).

Reddish pink form: IR (film, cm^{-1}) ν(CN) 2168 vs; ν(CO) 1883 vs (br).

Synthesis of $[Rh(CN\text{-}DMP\text{-}2,6)_4][Co(CO)_4]$ (3c). To a solution of $Co_2Rh_2(CO)_{12}$ (58.4 mg, 0.088 mmol) in 20 mL of *n*-hexane was added dropwise a solution of CN-DMP-2,6 (88.9 mg, 0.678 mmol) in 10 mL of hexane with stirring at room temperature. During the addition, a red-orange solid precipitated. The solid was recrystallized from CH_2Cl_2/*n*-hexane to give purple needle crystals of $[Rh(CN\text{-}DMP\text{-}2,6)_4][Co(CO)_4]$ (**3c**) in quantitative yield. One of the good needle crystals was submitted to single-crystal X-ray analysis (vide infra).

3c: Mp 135–137 °C. IR (CH_2Cl_2, cm^{-1}) ν(CN) 2146 vs; ν(CO) 1888 vs (br). ^1H NMR ($CDCl_3$) δ 2.40 (s, 24 H), 6.96–7.40 (m, 12 H). Anal. Calcd for $C_{40}H_{36}N_4O_4CoRh$: C, 60.16; H, 4.54; N, 7.02. Found: C, 60.26; H, 4.47; N, 7.25.

Reactions with Alkynes. Synthesis of $Co_2Rh_2(CO)_{10}(HC{\equiv}CR)$ (5a, R = Bu^n; 5b, R = Ph; 5c, R = SiMe$_3$). To a solution of $Co_2Rh_2(CO)_{12}$ (66 mg, 0.10 mmol) in 20 mL of *n*-hexane was added dropwise a solution of 1-hexyne (8.2 mg, 0.10 mmol) in 5 mL of *n*-hexane at room temperature under nitrogen. The solution was stirred at room temperature for 30 min. During the stirring the color of the solution gradually changed from brown to purple. The solvent was then removed in vacuo and the residue was redissolved in *n*-hexane and chromatographed on a silica gel column (*n*-hexane as eluant) to give $Co_2Rh_2(CO)_{10}(HC{\equiv}CBu^n)$ (**7**) in quantitative yield as a dark purple gum.

5a: IR (*n*-hexane, cm^{-1}) ν(CO) 2095 m, 2064 vs, 2047 s, 2030 vs, 1992 w (br), 1889 m. ^1H NMR ($CDCl_3$) δ 0.90 (m, 3 H), 1.28 (m, 4 H), 2.74 (m, 2 H), 8.85 (s, 1 H). ^{13}C NMR ($CDCl_3$) δ 13.7 (s), 22.5 (s), 37.9 (s), 55.1 (s), 149.5 (m, ≡CH), 176.8 (d, $J_{Rh\text{-}C}$ = 66 Hz, $RhCO_{eq}$), 177.7 (d, $J_{Rh\text{-}C}$ = 70 Hz, $RhCO_{eq}$), 187.8 (d, $J_{Rh\text{-}C}$ = 60 Hz, $RhCO_{ax}$), 188.7 (d, $J_{Rh\text{-}C}$ = 61 Hz, $RhCO_{eq}$), 193.5 (m, ≡CBu^n), 201 (br m, CoCO and μ-CO).

In the same manner, $Co_2Rh_2(CO)_{10}(HC{\equiv}CPh)$ (**5b**) and $Co_2Rh_2(CO)_{10}(HC{\equiv}CSiMe_3)$ (**5c**) were obtained as a dark purple solid in quantitative yield.

5b: IR (*n*-hexane, cm^{-1}) ν(CO) 2088 m, 2062 vs, 2043 vs, 2027 vs, 1985 w(br), 1890 m. ^1H NMR ($CDCl_3$) δ 7.10–7.25 (m, 5 H), 8.95 (s, 1 H). ^{13}C NMR ($CDCl_3$) δ 125.1 (s), 128.1 (s), 128.6 (s), 143.2 (m, ≡CH), 152.4 (s), 176.6 (d, $J_{Rh\text{-}C}$ = 66 Hz, $RhCO_{eq}$), 178.5 (d, $J_{Rh\text{-}C}$ = 68 Hz, $RhCO_{eq}$), 185.2 (m, ≡CPh), 187.6 (d, $J_{Rh\text{-}C}$ = 60 Hz, $RhCO_{ax}$), 188.5 (d, $J_{Rh\text{-}C}$ = 60 Hz, $RhCO_{ax}$), 201 (br m, CoCO and μ-CO).

5c: IR (*n*-hexane, cm^{-1}) ν(CO) 2095 m, 2063 vs, 2057 m, 2048 s, 2042 m, 2035 m (sh), 2027 vs, 2009 w, 1889 m. ^1H NMR ($CDCl_3$) δ 0.16 (s, 9 H), 9.32 (s, 1 H). ^{13}C NMR ($CDCl_3$) δ 1.8 (s), 163.5 (m, ≡CH), 175.7 (d, $J_{Rh\text{-}C}$ = 66 Hz, $RhCO_{eq}$), 179.9 (d, $J_{Rh\text{-}C}$ = 67 Hz, $RhCO_{eq}$), 183.2 (m, ≡$CSiMe_3$), 187.5 (d, $J_{Rh\text{-}C}$ = 61 Hz, $RhCO_{ax}$), 188.6 (d, $J_{Rh\text{-}C}$ = 62 Hz, $RhCO_{ax}$), 201 (br m, CoCO and μ-CO).

In spite of repeated attempts, satisfactory elemental analyses for **5a–c** have not been obtained, due to decomposition associated with recrystallization procedure, i.e., the drying process, from *n*-hexane. Therefore, the corresponding triphenylphosphine derivatives, $Co_2Rh_2(CO)_9(HC{\equiv}CR)(PPh_3)$ (**6a**, R = Bu^n; **6c**, R = $SiMe_3$) and $Co_2Rh_2(CO)_8(HC{\equiv}CR)(PPh_3)_2$ (**7a**, R = Bu^n; **7b**, R = Ph), were synthesized, which were fully characterized (vide infra).

Synthesis of $Co_2Rh_2(CO)_{10}(PhC{\equiv}CPh)$ (4b). The diphenylacetylene complex $Co_2Rh_2(CO)_{10}(PhC{\equiv}CPh)$ was synthesized by the literature procedure[8] with some modifications. To a solution of $Co_2Rh_2(CO)_{12}$ (66 mg, 0.10 mmol) in 25 mL of dichloromethane was added dropwise a solution of diphenylacetylene (18 mg, 0.10 mmol) in 5 mL of dichloromethane at room temperature under nitrogen. The solution was stirred for 1 h at room temperature; then the color of the solution became purple. The solution was concentrated in vacuo and submitted to purification by flash column chromatography on silica gel (eluant: *n*-hexane/CH_2Cl_2 = 2/1) affording $Co_2Rh_2(CO)_{10}(PhC{\equiv}CPh)$ (**4b**) in quantitative yield as a dark purple solid.

4b: IR (CH_2Cl_2, cm^{-1}) ν(CO) 2096 m, 2068 vs, 2060 vs (sh), 2029 s, 1878 m. ^{13}C NMR ($CDCl_3$) δ 127.0 (s), 127.7 (s), 128.2 (s), 151.7 (s), 175.8 (m, ≡CPh), 177.0 (d, $J_{Rh\text{-}C}$ = 77 Hz, $RhCO_{eq}$), 187.4 (d, $J_{Rh\text{-}C}$ = 60 Hz, $RhCO_{ax}$), 202 (br m, CoCO and μ-CO).

Synthesis of $Co_2Rh_2(CO)_9(HC{\equiv}CR)(PPh_3)$ (6a, R = Bu^n; 6c, R = SiMe$_3$). To a solution of $Co_2Rh_2(CO)_{12}$ (100 mg, 0.151 mmol) in 35 mL of *n*-hexane was added dropwise a solution of 1-hexyne (12.4 mg, 0.151 mmol) in 5 mL of *n*-hexane at room temperature under nitrogen. The solution was stirred at room temperature for 30 min. The IR spectrum of the mixture revealed the quantitative formation of $Co_2Rh_2(CO)_{10}(HC{\equiv}CBu^n)$. The solvent was then removed in vacuo, the residue was redissolved in *n*-hexane, and the insoluble material was filtered off. To this filtrate PPh_3 (40.1 mg, 0.151 mmol) in 10 mL of *n*-hexane was added dropwise. The solution was stirred at room temperature. After 2 h, the IR spectrum of the reaction mixture showed the presence of new bands, but bands due to $Co_2Rh_2(CO)_{10}(HC{\equiv}CBu^n)$ still remained. A TLC analysis of the reaction mixture showed two new spots corresponding to the monosubstituted (major) and disubstituted (minor) complexes. The reaction was then stopped and the reaction mixture was concentrated and chromatographed on a silica gel column. A purple band, eluted with *n*-hexane/CH_2Cl_2 (4/1), gave $Co_2Rh_2(CO)_9(HC{\equiv}CBu^n)(PPh_3)$ (**6**) as a dark purple solid. Single crystals of **6a** were obtained by slow cooling of a saturated *n*-hexane solution, one of which was submitted to single-crystal X-ray analysis (vide infra).

6a: IR (CH_2Cl_2, cm^{-1}) ν(CO) 2073 s, 2027 s, 2000 vs (br), 1890 w (sh), 1859 s. ^1H NMR ($CDCl_3$) δ 0.88 (t, J = 7.1 Hz, 3 H), 1.25 (m, 4 H), 2.61 (m, 2 H), 7.44–7.66 (m, 15 H), 8.12 (d, $J_{P\text{-}H}$ = 19.5 Hz, 1 H). ^{13}C NMR ($CDCl_3$) δ 13.8 (s), 22.5 (s), 37.9 (s), 54.5 (s), 128.8 (d, $J_{P\text{-}C}$ = 10.4 Hz, $C_{3,5}$ of PPh_3), 131.1 (s, C_4 of PPh_3), 131.7 (d, $J_{P\text{-}C}$ = 42.4 Hz, C_1 of PPh_3), 133.4 (d, $J_{P\text{-}C}$ = 10.9 Hz, $C_{2,6}$ of PPh_3), 158.4 (br d, $J_{P\text{-}C}$ = 14.0 Hz, ≡CH), 179.5 (dd, $J_{Rh\text{-}C}$ = 72.6 Hz, $J_{P\text{-}C}$ = 41.0 Hz, $RhCO_{eq}$), 189.6 (d, $J_{Rh\text{-}C}$ = 59.2 Hz, $RhCO_{ax}$), 191.1 (dd, $J_{Rh\text{-}C}$ = 60.6 Hz, $J_{P\text{-}C}$ = 12.0 Hz, $RhCO_{ax}$), 196.5 (br d, $J_{P\text{-}C}$ = 13.9 Hz, ≡CBu^n), 207 (m, CoCO and μ-CO). Anal. Calcd for $C_{33}H_{25}O_9PCo_2Rh_2$: C, 43.07; H, 2.74. Found: C, 43.14; H, 2.77.

In the same manner, $Co_2Rh_2(CO)_9(HC{\equiv}CSiMe_3)(PPh_3)$ (**6c**) was obtained as a dark purple solid.

6c: IR (*n*-hexane, cm^{-1}) 2070 m, 2042 sh, 2035 s, 2026 s, 2007 sh, 2002 s, 1893 (br) m, 1857 (br) mw. ^1H NMR ($CDCl_3$) δ 0.05 (s, 9 H), 6.68–7.75 (m, 15 H), 8.55 (d, J_{P-H} = 20.1 Hz, 1 H). Anal. Calcd for $C_{32}H_{25}O_9PSiCo_2Rh_2$: C, 41.05; H, 2.69. Found: C, 40.97; H, 2.91.

Synthesis of $Co_2Rh_2(CO)_8(HC{\equiv}CR)(PPh_3)_2$ (7a, R = Bu^n; 7b, R = Ph). First, the synthesis of **5a** was carried out as described above and to its solution in *n*-hexane was added dropwise an excess of PPh_3 (157 mg, 0.600 mmol). A precipitate was formed during the reaction. After stirring for 2 h at room temperature, a TLC analysis of the reaction mixture showed a major spot corresponding to the disubstituted cluster. The solvent was removed in vacuo and the residue was dissolved in dichloromethane. Concentration of the reaction mixture in vacuo and purification by a flash column chromatography on silica gel (eluant: *n*-hexane/CH_2Cl_2 = 2/1) afforded $Co_2Rh_2(CO)_8(HC{\equiv}CBu^n)(PPh_3)_2$ (**7a**) as a purple solid.

7a: IR (CH_2Cl_2, cm^{-1}) ν(CO) 2050 m, 2016 w (sh), 1988 s (sh), 1976 vs, 1867 m, 1837 m. ^1H NMR ($CDCl_3$) δ 0.58 (t, J = 7.1 Hz, 3 H), 0.82 (m, 2 H), 1.01 (m, 2 H), 2.29 (m, 2 H), 7.47 (m, 18 H), 7.69 (m, 12 H), 8.65 (d, J_{P-H} = 21.8 Hz, 1 H). ^{13}C NMR ($CDCl_3$) δ 13.5 (s), 22.5 (s), 37.1 (s), 52.8 (s), 128.5 (m, $C_{3,5}$ of PPh_3), 130.7 (s, C_4 of PPh_3), 132.2 (d, J_{P-C} = 41.9 Hz, C_1 of PPh_3), 133.1 (d, J_{P-C} = 40.4 Hz, C_1 of PPh_3), 133.6 (d, J_{P-C} = 10.6 Hz, $C_{2,6}$ of PPh_3), 134.0 (d, J_{P-C} = 10.9 Hz, $C_{2,6}$ of PPh_3), 157.6 (d, J_{P-C} = 15.4 Hz, $\equiv$CH), 189.2 (dd, J_{Rh-C} = 59.1 Hz, J_{P-C} = 10.3 Hz, $RhCO_{ax}$), 191.6 (dd, J_{Rh-C} = 59.0 Hz, J_{P-C} = 10.6 Hz, $RhCO_{ax}$), 197.6 (d, J_{P-C} = 15.3 Hz, $\equiv CBu^n$), 214.8 (m, CoCO and μ-CO). Anal. Calcd for $C_{50}H_{40}O_8P_2Co_2Rh_2$: C, 52.02; H, 3.49. Found: C, 52.40; H, 3.60.

In the same manner, $Co_2Rh_2(CO)_8(HC{\equiv}CPh)(PPh_3)_2$ (**7b**) was obtained as a dark purple solid. **7b**: IR (*n*-hexane, cm^{-1}) 2076 s, 2047 vs, 2031 s, 2024 s, 2011 m, 1889 (br) m, 1860 (br) mw. ^1H NMR ($CDCl_3$) δ 6.75–7.75 (m, 35 H), 8.26 (d, J_{P-H} = 18.9 Hz, 1 H). Anal. Calcd for $C_{45}H_{36}O_8P_2C_2Rh_2$: C, 49.57; H, 3.32. Found: C, 49.06; H, 3.39.

X-ray Crystal Structure Determination of $[Rh(CN\text{-}DMP\text{-}2,6)_4][Co(CO)_4]$ (3c) and $Co_2Rh_2(CO)_9(PPh_3)(HC{\equiv}CBu^n)$ (6). A single crystal selected for intensity measurements was placed, encased in mineral oil, inside a thin-walled glass capillary. The crystal was then optically centered on an Enraf-Nonius CAD4 diffractometer controlled by a Digital PDP 8/e computer and equipped with a graphite monochromator and Mo Kα radiation.

For **3c**, a monoclinic unit cell was derived by least-square refinement of 25 of the strongest high-angle reflections. The space group $P2_1/c$ was assumed and confirmed by the successful solution and refinement of the structure. During the data collection, three strong standard reflections were used as intensity controls and checked every hour, and two standard reflections were used as orientation control and checked every 100 reflections. The structure was solved on a Vax station 3100 computer using the Texray structure-solving program. A Patterson map was solved to locate the positions of both rhodium and cobalt atoms. The positions of the aromatic hydrogen atoms were assigned by using standard C-H bond parameters. Methyl hydrogens on the phenyl rings were located on a difference Fourier map after refinement of the structure. All non-hydrogen atoms except aromatic moieties were refined anisotropically. The R value is 0.032 (R_w = 0.039). Difabs empirical absorption correction was applied to the data.

In a similar manner, a triclinic unit cell was derived for **6**. The space group $P\bar{1}$ was assumed and confirmed. The structure was solved on a Vax 780 computer using the Texray structure solving program. A Patterson map was solved to locate the position of one of the rhodium atoms. Refinements of subsequent electron density difference maps revealed the location of the other non-hydrogen atoms. The positions of the hydrogen atoms were assigned by using standard C–H bond parameters, except for the hydrogen on the acetylenic carbon, H25, which was located from its Fourier peak after the structure refinement. All non-hydrogen atoms were refined anisotropically to give an R value of 0.051 (R_w = 0.063). Difabs empirical absorption correction was applied to the data.

Acknowledgment. This research was supported by grants from National Science Foundation, National Institute of Health (NIGMS), and the donors of Petroleum Research Fund, administered by the American Chemical Society. The authors are grateful to Mr. John Franolic, Department of Chemistry, SUNY at Stony Brook, for the X-ray crystallographic analyses.

Supplementary Material Available: Listings of additional bond lengths and angles, hydrogen atom parameters, and anisotropic thermal parameters and additional drawings of **3c** and **6** and a least-squares planes table for **6** (39 pages); listings of the observed and calculated structure factors (60 pages). Ordering information is given on any current masthead page.